Smart Materials and Structures

PAPER • **OPEN ACCESS**

A soft gripper with programmable effective length, tactile and curvature sensory feedback

To cite this article: Yufei Hao *et al* 2020 *Smart Mater. Struct.* **29** 035006

View the article online for updates and enhancements.

This content was downloaded from IP address 106.39.42.116 on 01/07/2020 at 10:05

OPEN ACCESS
IOP Publishing
Smart Materials and Structures
Smart Mater. Struct. **29** (2020) 035006 (11pp)
https://doi.org/10.1088/1361-665X/ab6759

A soft gripper with programmable effective length, tactile and curvature sensory feedback

Yufei Hao[1,3], Zemin Liu[1,3], Jiaqi Liu[1], Xi Fang[1], Bin Fang[2], Shilin Nie[1], Yingchun Guan[1], Fuchun Sun[2], Tianmiao Wang[1] and Li Wen[1]

[1] Department of Mechanical Engineering and Automation, Beihang University, Beijing, People's Republic of China
[2] Department of Computer Science and Technology, Tsinghua University, Beijing, People's Republic of China

E-mail: liwen@buaa.edu.cn

Received 10 June 2019, revised 17 November 2019
Accepted for publication 3 January 2020
Published 27 January 2020

Abstract

Soft grippers based on fluidic elastomer actuators have the characteristics of gentle and adaptable grasping that is difficult to realize by rigid grippers. However, it remains challenging to implement a compact gripping device that has multiple bending configurations to exert appropriate force, and sensory capabilities to evaluate the grasping state. Here, we present a soft gripper with variable effective lengths (VELs) that is achieved by rapidly softening selective shape memory polymer sections (within 0.6 s) via a flexible heater. A vortex tube is used to jet cold airflow to accelerate the stiffening process (within 14 s). We show that the soft gripper can not only identify objects but also exert higher gripping force by setting appropriate length according to pneumatic-thermal hybrid actuation. We further propose a touch-reconfiguration-grasp strategy to showcase the synergy of VELs and sensory feedback. The gripper first touches the object under the fully softened state and evaluates the grasping condition based on the sensors' feedback, then reconfigures the bending length and grasps the object until successful. We envision that soft grippers with sensing ability and reconfigurable grasping configurations would be promising for future applications in unconstructed environments.

Supplementary material for this article is available online

Keywords: shape memory polymer, variable mechanical configuration, liquid metal, soft gripper

(Some figures may appear in colour only in the online journal)

1. Introduction

Grippers, which are indispensable to liberate the labor force, are always a research hotspot to the scientific and engineering communities. Conventional rigid grippers may yield high local stress while contacting objects, and make it difficult to control while grasping an object [1, 2]. Recently, advances in smart materials boost the research of soft robotic grippers [3]. For example, dielectric elastomers are exploited in the design of soft grippers such as the DEMES gripper [4] and the wrapping gripper [5]. Low melting point alloys [6] and shape

[3] These authors contributed equally to this paper.

Original content from this work may be used under the terms of the Creative Commons Attribution 4.0 licence. Any further distribution of this work must maintain attribution to the author(s) and the title of the work, journal citation and DOI.

memory polymers (SMPs) [7, 8] enable variable stiffness of the grippers via the phase transition effect. Magnetic-actuated [9, 10], thermally activated [11], solution stimulated [12, 13], and light-responsive [14] materials endow the grippers with untethered and microscale features. In addition, the self-healing material enables soft grippers with recovering ability while encountering damage, cuts, and perforations caused by sharp objects [15]. Other micro grippers based on piezo-electric stack actuators or voice coil actuators are also developed [16–18].

Soft grippers based on fluidic elastomer actuators (FEAs) have the properties of low-cost, environmental robust and easy fabrication [19, 20]. These properties make the FEA based grippers suitable for uncertain, dynamic task environments, including safe human-robot interactions. They have several promising applications including pick-place tasks [21], wearable devices [22], and underwater biological sampling [23, 24]. Soft sensors including the stretchable optical waveguides [25], the magnet hall sensor [26], the fabric capacitive sensor [27], and liquid metal sensors [28, 29] are developed, which can be integrated into FEA grippers to provide feedback during grasping. Recently, the soft gripper with somatosensory feedback further enriches the gripper's functionality in terms of innervating the gripper with multiple conductive features [30]. Besides soft sensors, variable stiffness mechanisms are deployed to improve the load capacity [31, 32], and multiple degrees of freedom paradigms are explored to enrich the multimodal kinematics [33–35]. Despite these research advances, we imagine that implementing a gripper that can change its grasping space to exert appropriate force on objects with different shapes/sizes under the instruction of sensory feedback, would further improve the grasping performance and dexterity of the soft gripper. Hear, the grasping space means the space between the fingers of the gripper when the fingers move during operation. To this end, the design and fabrication of a compact soft gripper with variable effective length (VEL), sensory feedback, and reconfigurable grasping are essential.

Here we proposed a new design to change the grasping space of the soft grippers by embedding the SMP, which functionalizes as a VEL layer, into the FEA. The VEL can be operated online by selectively heating different sections of the layer via a laser-cut thin heater. Only the heated sections can be softened, thus can be bent under pressurization. To accelerate the cooling of SMP, we used a vortex tube that can blow cold airflow to the VEL layer. Systematic experiments were conducted to test the effect of the VEL on the gripping force on objects of different sizes. To endow sensory feedback, we embedded an EGaIn curvature sensor at the actuator's backbone and an EGaIn tactile sensor at its fingertip. We conducted experiments to verify whether the gripper can identify objects with sensory feedback. Finally, we proposed a touch-reconfiguration-grasp strategy to show that the gripper can autonomously select proper effective lengths to achieve improved grasping.

2. Design and fabrication

The design of the soft actuator with the VEL layer and the soft sensors is shown in figure 1(a). The actuator is composed of the soft upper layer, the VEL layer, and the tactile sensor layer. The upper layer (made of Dragon Skin 20, Smooth on. Inc., USA) is a corrugated structure with an EGaIn curvature sensor located at the top. The curvature sensor is a silicone rubber beam inside which is a two-line microchannel infused with EGaIn. When the actuator bends, the microchannel is stretched and the cross-section area is decreased, which leads to the resistance change of EGaIn. By applying a constant current to the leads of the microchannel, we can measure the variation of the resistance. After calibration, we can use the resistance of the sensor to predict the curvature of the actuator under different effective lengths. To enhance the sensibility of the curvature sensor, we embed it to the back of the upper layer where it can be stretched to the maximum. The tactile sensor on the tip of the actuator is a spiral-shaped, single-pixel pressure sensor for providing feedback to the contact force when the actuator touches an object [36] (figure 1(b)). With a similar principle to the curvature sensor, the dimension change of the microchannel of the tactile sensor under external pressure results in the resistance change of EGaIn. After calibration, we can use the resistance of the sensor to predict the normal force pressure. The VEL layer is made of the SMP epoxy compound, EPON 828 (Hexion Inc., USA) and Jeffamine D400 (Huntsman Polyurethanes Ltd, China) with a ratio of 10:4 by weight. To fabricate this layer, we first mix the two materials in a paper cup, then pour the mixture to fill half of the silicone rubber mold and let it sit for about 24 h to release the bubbles and increase the viscosity. After curing the material in the oven at 70 °C for six hours, we put the heater on top of it and pour the uncured mixture to fill the mold and cured it once again. To achieve multiple mechanical configurations of the actuator, three separate heating sections (sections 1–3) are designed in our current VEL layer (figure 1(b)).

The manufacturing process of the actuator prototype is shown in figures 1(c) and (d). The heater determines the phase transition speed of the VEL layer, and it should be flexible enough to avoid any mechanical influence on the bending of the actuator. Therefore, we fabricated a flexible, thin constantan foil (5 μm in thickness) heater via a high-resolution focused picosecond laser beam with 600 PS pulses at 200 kHz repetition rate with a central wavelength of 1064 nm (figure 1(c)), which is produced by the laser system (PicoYL-15-0.1, Anyang Laser Technology Co., Ltd, China). The constantan foil was chosen because of its high electrical resistivity (5.0 × 10-7 Ω·m), which enables high electro-heat conversion, and it is commercially available. After cutting the designed pattern on the foil (the pattern is shown in figure S1 is available online at stacks.iop.org/SMS/29/035006/mmedia) and soldering the copper wire to the pads of the heater, we embedded the heater inside the SMP material to construct the entire VEL layer. The laser cutting method is adopted here due to the following reasons: (1) it does not require high-cost fabrication machines and the ultra-clean

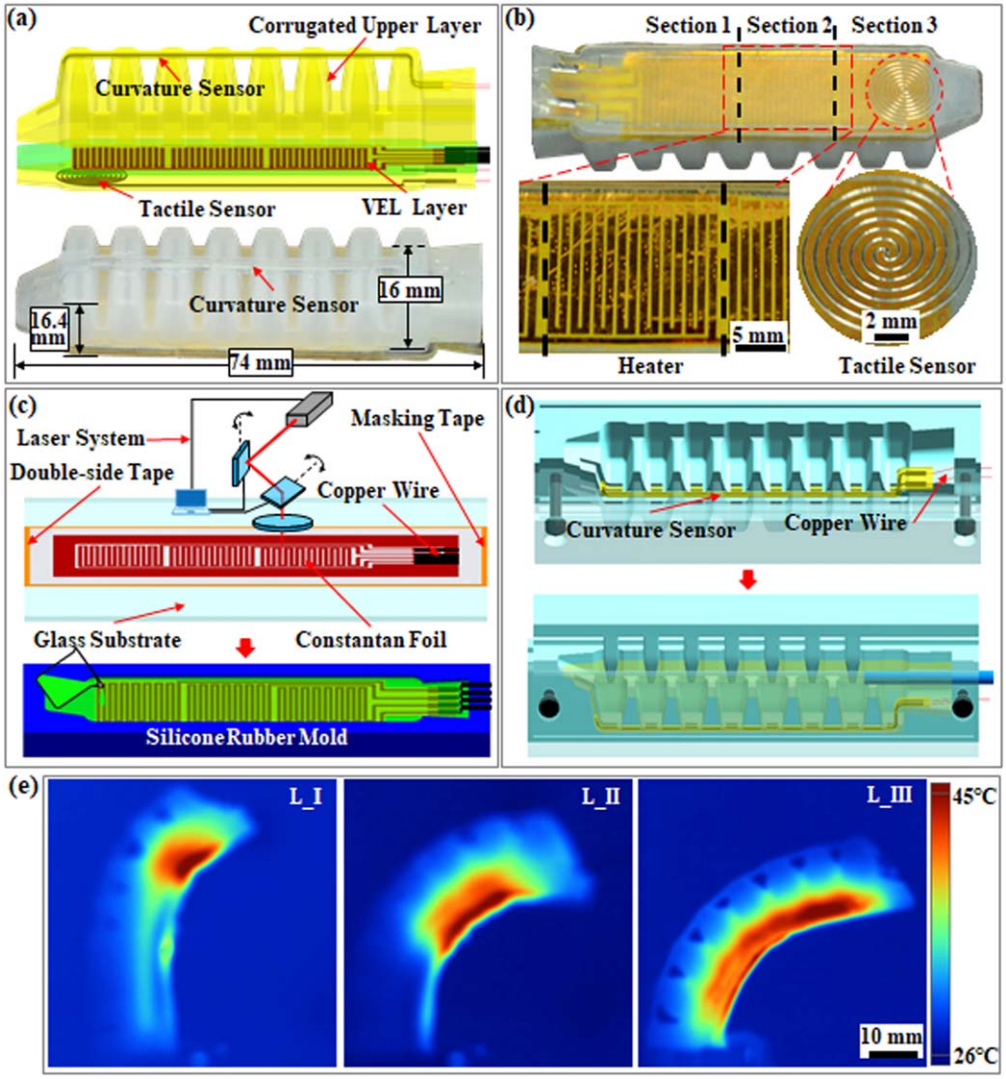

Figure 1. The design and fabrication of the multi-material integrated soft actuator. (a) The actuator is composed of a corrugated pneumatic silicone upper layer, a variable effective length (VEL) layer, and a tactile sensor layer. The total height, width, and length of the actuator are separately 16.4, 16 and 74 mm. The EGaIn curvature sensor, with a thickness of 0.8 mm and a width of 2mm, is at the top of the pneumatic silicone layer to give feedback to the curvature information. The EGaIn tactile sensor, with a thickness of 0.8 mm, is under the tip of the VEL layer to perceive the force. Both the curvature sensor and tactile sensor have a microchannel filled with EGaIn, with a cross-section demotion of 0.3 and 0.3 mm. The heater, with a thickness of 5 μm, is embedded inside the non-conductive VEL layer to speed up the phase transition time. The thickness of the VEL layer is 2 mm. The different colors represent different materials: yellow represents the silicone rubber; green represents the SMP which was used to construct the VEL layer; red represents the cooper foil heater and dark gray represents EGaIn. (b) The snapshots of the real prototype. The heater has three sections so it can separately soften different sections of the VEL layer to change the bending lengths. (c) The rapid fabrication process of the VEL layer. Before laser cutting, a masking tape (124 μm thick) which functions as the substrate of the flexible heater adhered to the glass substrate, then a double-sided tape (109 μm thick) was affixed to the masking tape. After that, the constantan foil (5 μm thick) was adhered to the upper side of the double-sided tape to reduce the thermal distortion during laser cutting. After laser cutting, the heater was transferred from the substrate to the half cured VEL layer inside the silicone rubber mold, and an uncured composite was poured on the top of the heater to construct the entire VEL layer. The layer was covered with a glass substrate during curing to ensure a smooth surface. (d) The curvature sensor integration process. First, we put the curvature sensor in the dent of the mold and pre-stretched it to avoid buckling when bending it to the outside, then uncured silicone rubber was poured in the mold to make the upper layer. (e) The infrared pictures show the three VELs of the actuator. L_I: soften section 1 shown in (b); L_II: soften sections 1 and 2; L_III: soften sections 1–3. All the VELs can be softened within 0.6 s with a current of 1 A.

room environment [37]; (2) the heater layer can be fabricated within 10 s, with no need for a longtime substrate preparation and post-etching processing as required by the metal deposition method [37]; (3) The substrate (masking tape) is porous, therefore the liquid SMP compound can penetrate into the tape and guarantee a firm connection between the heater and the SMP. The heater is embedded in the middle of the VEL layer (figure 1(c)). This design allows the heat to transmit to both sides of the VEL layer and increases the phase transition speed. To embed the curvature sensor on the top of the upper layer, the prepared sensor was first stretched and put in the dent of the two fastened symmetrical models before the uncured silicone rubber was poured into the models (figure 1(d)). In the final step, the three parts of the actuator

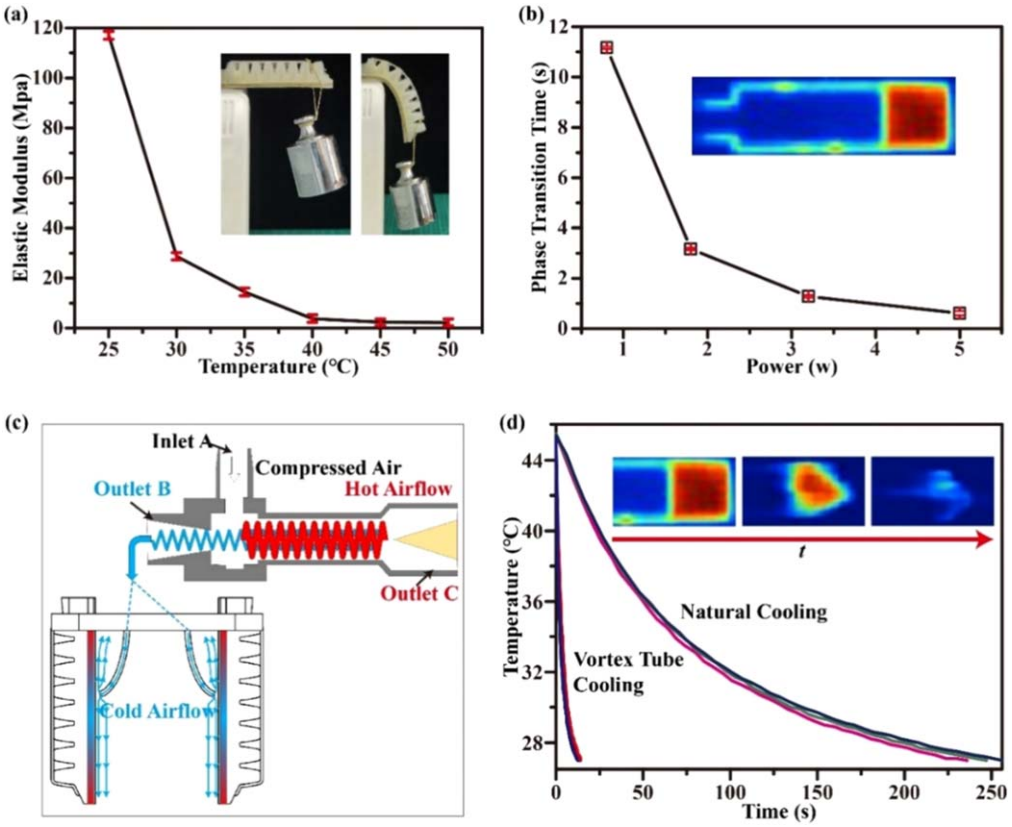

Figure 2. Mechanical and thermal properties of the VEL layer. (a) The elasticity modulus of the layer under different temperatures. The inserted panels show that the actuator can support a weight of 200 g at the rigid state (25 °C) without bending, but it can be bent by the gravity of the weight at the soft state (45 °C). (b) The phase transition time as a function of the input power. The inserted infrared image shows that the heat does not propagate from the heated section to the unheated section. (c) The principle of the vortex tube used to shorten the cooling time. (d) The cooling time of the layer in its natural condition and using the vortex tube. The inserted infrared images show the temperature changing when we cool down the VEL layer using the vortex tube.

were glued together in order via the use of superglue (QIS-3009, Dongguan JingDa Adhesive Co., Ltd, China). By heating different sections of the VEL layer via the flexible heater (figure 1(b)), the corresponding sections will be softened, and thus can be bent when pressurizing the upper layer, while the unheated sections remain straight (figure 1(e)). Therefore, we can adjust the VEL to actively alter the grasping space of the gripper according to such a pneumatic-thermal hybrid actuation approach, which is different from the traditional pneumatic-only strategy. The infrared photos of changing the effective lengths (L_I, L_II and L_III) are shown in figure 1(e).

3. Results and discussion

3.1. Mechanical and thermal properties of the actuator

We tested the elastic modulus of the VEL layer under different temperatures (shown in figures 2(a) and S2). At 25 °C, the elastic modulus is about 120 MPa. When the VEL layer is heated to 30 °C, the elastic modulus decreases sharply. Over the glass transition temperature (44 °C), the value reduces to 2 MPa; further increasing the temperature leads to non-significant stiffness changes. The elastic modulus of the rigid state is about 60 times that of the soft state, which guarantees that the actuator can hold a 200 g weight at the rigid state (the inserted pictures in figure 2(a)). Noted that the temperature difference between the two states is about 20 °C, which requires less time and power to achieve the phase transition. The phase transition time with the relationship of input power is depicted, and the phase transition time decreases as the power increases (figure 2(b)). Here the phase transition time is defined as the time needed to heat the VEL layer from room temperature (26 °C) to the glass transition temperature (44 °C). The inserted infrared picture (figure 2(b)) shows a uniform temperature distribution in the heated section and a distinct gap between the heated and the unheated sections. Notably, the time could be limited to about 0.6 seconds (also shown in supplementary video S1) when the power reaches 5 W.

Here we attempt to reduce the cooling time of the prototype by using a compact-sized, low-cost, widely available vortex tube (NaiLiShi, Shenzhen RuiJie Technology Co., Ltd, China) (figures 2(c), S6). Applying the compressed air from the inlet A, cold air can be expelled from outlet B with a flow speed of 37.6 mm s^{-1} (while hot air can be released through outlet C). As shown in figure 2(d), blowing the cold air to the surface of the VEL layer, the cooling time of the VEL layer was reduced to about 14 s (also shown in supplementary

video S2), much faster than the natural cooling which could take about 240 s. Therefore, the thermal convection between the VEL layer and the environment is significantly enhanced, and the cooling time is consequently reduced. The infraed pictures in figure 2(d) show the changing of the temperature under vortex cooling. Noted that, the long cooling time of SMPs is always a dilemma that hinders their further application. Compared to the water cycling cooling which needs a circulating system for liquids [38], our proposed cooling method (via a vortex tube) is compact and practical for applications.

3.2. VEL for grasping

A suitable finger length of the soft gripper for a specific object can improve the grasping performance. Here, we propose a VEL method to change the grasping space to increase the contact area based on the size of the objects. For example, when grasping a large object, the gripper with a longer length can exert more grasping space to enclose it than that with a shorter length (upper panels in figure 3(a)). In contrast, while grasping a small object, the gripper using a shorter effective length can have more contact area compared to the configuration using a longer length (lower panels in figure 3(b)). Systematic force measurements were also conducted to verify this. As shown in figure 3(b), the pull-off forces of the gripper vary with the size of the grasped objects and the effective lengths of the actuator, even if the gripper is inflated with the same pressure. Here the pull-off force is defined as the maximum force generated during the detaching process (see pull-off force test in the experimental section). For the small-sized cylinder (38 mm in diameter), the maximum pull-off force is generated when L_I is used. For the middle-sized cylinder (48 mm in diameter), the maximum force comes from L_II. The large-sized cylinder (58 mm in diameter) can only be grasped by using L_III. And all the maximums appear when the grasping space of the gripper is closest to the size of the objects. Figure 3(c) shows the force change while the gripper is gradually detaching from the three different sized cylinders under the effective length L_III. For all the three objects, the forces increase gradually, then decrease. However, the peak value of the biggest object is greater than the others. Figure 3(d) shows that the forces also perform an increasing-decreasing trend when the gripper is gradually detaching from the middle-sized object for all of the three effective lengths. Moreover, the L_II, which can form a similar enclosing profile with the object, is the one that can produce the largest pull-off force. Based on the results of figures 3(b)–(d), we conclude that the gripper could produce more grasping force when its grasping space is similar to the size of the object. Furthermore, the inserted pictures in figure 3(e) show that the gripper can have more contact area with the objects (ink bottle, orange and Rubik's cube) by selecting proper effective lengths. Therefore, changing the VELs of the gripper for objects of different sizes can improve grasping performance.

Our designed VEL layer and corresponding flexible heaters endow the gripper with the ability to automatically change the grasping modes. We propose to change the effective length of the actuator by heating different sections of the VEL layer, rather than replacing different actuators or manually changing the actuator length [21], which guarantees the simplicity and autonomous of the entire actuator system. Compared to the soft elastomer grippers with a constant bending curve [20], our actuator can configure to an appropriate effective length to grasp different objects and generate a larger gripping force. Besides, the fast heating and cooling methods guarantee the efficiency of the gripper, which paves a way for future practical applications.

3.3. The sensory capacity of the actuator

The resistance of the curvature sensor with the relationship of inflated air pressure is characterized in figure 4(a). For all the three VELs, $\Delta R/R$ increases with the inflating pressure. While under the same pressure, $\Delta R/R$ intensifies with the increased effective length of the actuator. Although the actuator only has one curvature sensor, the results show that the sensor provides the actuator with the ability to differentiate the bending curvature and the VEL configurations on the prerequisite that the inflated pressure is defined. We also tested the dynamic response of the curvature sensor and found that the curvature sensor keeps pace with the step increase/decrease of the inflated pressure (figure S3(a)). The output voltage has a little shift with the air pressure during the pressurization and depressurization process. We suppose this mismatch may be induced by the viscoelasticity of the elastomer material as well as the compressibility of the air pressure. The repeatability of the sensor under the instantaneous inflation-deflation cycle performs well (figure S3(b)).

The resistance change of the tactile sensor is characterized in figure 4(b). As the results show, $\Delta R/R$ increases with the normal force pressure and shows a small bias under different pressures. Further increasing the resolution of the sensor's microchannel would raise the resolution of sensing [39]. We found that temperature has a minor influence on the resistance of the sensor (figure S4(a)). When heating the sensor from 25 °C to 45 °C, the resistance increased by 2.5%, which is acceptable while grasping and bearing the external force. For the dynamic response test of the tactile sensor when attached to the actuator, we can see the sensor performs differently under the freeload and load conditions (figure S4(b)). The tactile sensor has slight hysteresis when the actuator is inflated under the load condition (figure S4(b)), but with acceptable repeatability (figure S4(c)).

With the participation of external movements via a robot arm (MOTOMAN MH3F, YASKAWA Inc., Japan), we demonstrated the potential of a simple two-fingered gripper (with all three VEL sections softened) identifying 2D and 3D shaped objects as a step towards sensing soft grasping without visual feedback. The method is based on the hypothesis that the curvature of the actuator when the gripper touches an object is less than that in free bending under the same inflated pressure. We exhibited the method by using the gripper to recognize a dog-bone shaped cuboid (figure 4(c)) and a gourd (figure 4(d)). For the dog-bone shaped cuboid, we first moved

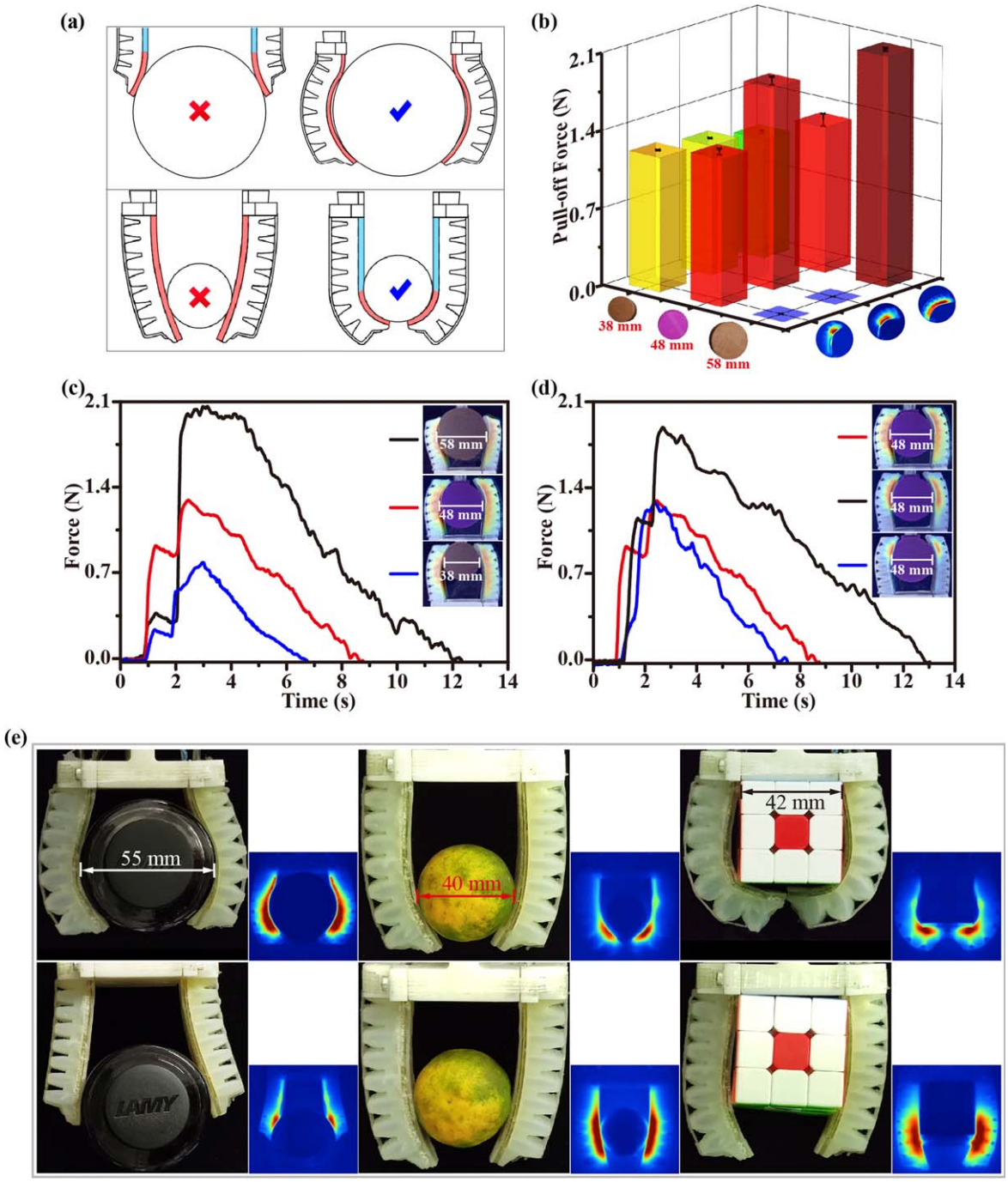

Figure 3. The force results of the gripper under different VEL configurations. (a) The sketches show the importance of adjusting the effective length when grasping objects of different sizes. (b) The pull-off force as a function of the size of the objects and the VELs of the gripper. The diameters of the three cylinders are 38 mm, 48 mm, and 58 mm respectively. The inflating pressure for all the cases is 40 kPa. (c) The force results when the gripper grasps objects of different sizes using the same gripper setting (L_III). (d) The force results when the gripper grips the same object using different VELs (L_I, L_II, and L_III). (e) Images show that the gripper can encompass the objects better by setting a proper effective length to adjust the grasping space in line with the size of the objects. The infrared images indicate which effective length the gripper uses.

the robot arm all the way to one end of the object and pressurized the actuator (30 kPa), the curvature sensor data was recorded as the reference data at this point. Then the gripper was deflated, and the robot arm was moved along the chord length of the cuboid. At each sliding step (18 mm), the gripper was inflated with the same pressure (30 kPa) and pinched the object, and the difference between the current sensor data and the reference data (sensor data under free bending state) was recorded. As shown in figure 4(c), the data plotting on the ΔV-displacement 2D coordinate shows a similar shape to that of the physical object according to the 'slide-and-pinch' approach.

For the three-dimensional gourd, the robot arm moved to the top of the object and the gripper executed a free bending

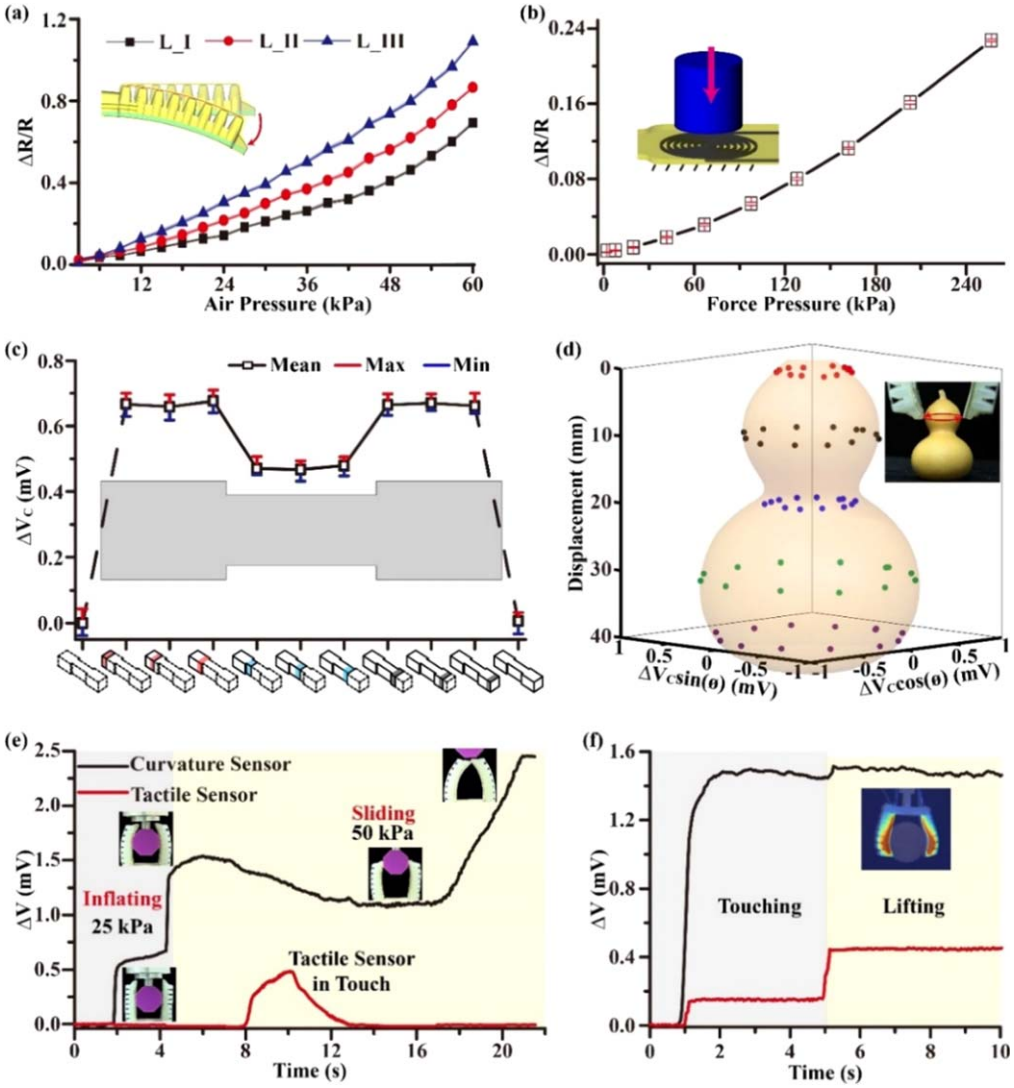

Figure 4. Results of the sensory feedback. (a) The resistance variation of the curvature sensor as a function of air pressure under different VELs. (b)The resistance changing of the tactile sensor as a function of normal pressure. (c) The feedback of the curvature sensor when the gripper tried to recognize the shape of the dog-bone shaped cuboid with the assistance of a robot arm. For this experiment, the full-length gripper bent to touch the object after the robot arm moved every 18 mm along the length of the object. ΔV_C indicates the voltage changing for the curvature sensor. (d) The feedback of the curvature sensor when the full-length gripper tried to reproduce the shape of the gourd. For this experiment, the gripper touched the gourd after the robot arm rotated every 30°. Also, the robot arm moved down 10 mm after it rotated 180°. (e) The feedback of the curvature sensor and tactile sensor while the gripper was touching and sliding over the surface of the octagonal prism with length L_II. The gray area shows the inflating period while the yellow area shows the sliding process. (f) The feedback of the two sensors while the gripper was lifting the big cylinder with a weight of 100 g and a diameter of 58 mm.

and recorded the reference data. Then the robot arm moved down 10 mm, and the gripper performed a pinch motion (under pneumatic pressure of 30 kPa) and recorded the data upon every 30° (rotated by the robot arm). After recording data for an entire circle, the robot arm further moved down (with a step of 10 mm) to perform the 'rotary-pinch' at each local height of the gourd. The sensory data was shown in figure 4(d), and the data plotting on the 3D coordinate shows a similar shape to that of the physical objects. The whole identification processes of the above two objects (the dog-bone shaped cuboid and the gourd) were separately demonstrated in supplementary video S3 and S4.

To fully demonstrate the utility of both bending and tactile sensory feedback, we mounted the two-fingered gripper and tested the sensing ability when the grasped objects sliding along the gripper (mimicking the falling or removing of a grasped object). As shown in figure 4(e) and supplementary video S5, when the gripper is inflated with 25 kPa and contacts the octagonal prism at ∼2 s, the curvature sensory data increases rapidly (0.6 mV). Further increasing the pressure to 50 kPa (∼4s), the gripper fully embraces the object and the bending sensor value increases about 1.54 mV. When the sliding process starts, the distance between the two fingertips gradually increases when the gripper slides across the upper part of the prism, the curvature sensor value slightly descents from 1.54 to 1.1 mV (∼5 to ∼13 s). When the gripper touches the vertical surface of the object (from ∼13 to ∼16 s), the curvature sensor value remains constant as the

distance between the two fingertips is constant. Finally, the gripper gradually detaches from the object, the curvature sensor increases consequently. During the sliding process, the tactile sensor starts to respond from ∼8 s due to the contact of the fingertip to the object and reaches up to 0.5 mV at ∼10 s, returns to 0V when the fingertip lose contact with the object at ∼12 s. The octagonal prism is pulled completely away from the gripper at ∼21 s while the inflation pressure is maintained, the curvature sensor value retains (2.4 mV). We also provide the sensory data when a cylinder object slid over the gripper (figure S5(a)). We found that gripping objects with different shapes or contours would induce significantly different bending curvature and tactile sensory feedback (supplementary video S6). Through these tests on mimicking the kinesthetic nature of falling (or removing) an object from the inflated gripper, we can clearly observe how the curvature and tactile sensing change with time, and the objects' contour.

We also tested the responses of the two sensors while the gripper was lifting objects. In figure 4(f), when the gripper is inflated with a pressure of 50 kPa and embraces the cylinder-shaped object (58 mm in diameter and 100 g in weight) at ∼1 s, both the curvature sensor and tactile sensor increase immediately, then remain constant after fully embracing the object. At ∼5 s, the gripper starts to lift the object, the tactile sensory value increases significantly, while the curvature sensory value increases slightly. After the object is completely lifted up, the two sensory values remain constant. We also show that the two sensors output different values when the gripper lifts a cylinder-shaped object with a smaller size and weight (figure S5(b)). Since the curvature sensor data changes with the size, and the tactile sensor data changes with the weight, the gripper can automatically sort out the smaller cylinder based on the disparity of the sensory feedback (supplementary video S7).

3.4. Reconfigurable grasping based on sensory feedback

To achieve improved grasping autonomously, we propose a touch-reconfiguration-grasp strategy that utilizes the feedback of both curvature and tactile sensors to set an appropriate effective length for a specific sized object. The general idea is to probe both the embrace curvature and the fingertip contact thus to guide proper effective length setting, such that the gripper is able to robustly grip and lift the object. The flowchart of the strategy is shown in table 1. To determine whether a grasp is successful, we defined some parameters. ΔV_C is defined as the curvature sensor data during grasping, minus that in free bending under the same inflated pressure. ΔV_F is defined as the tactile sensor data increase during grasping. Under free bending state without touch an object, ΔV_C and ΔV_F are zero. During grasping, $\Delta V_C < \delta_1$ (a threshold based on the deviation of the sensor during calibration) means the gripper embraces the object, and $\Delta V_F > \delta_2$ (also a threshold based on the deviation) means the fingertip touches the object. We only consider $\Delta V_C < \delta_1$ and $\Delta V_F > \delta_2$ as a successful grasping. Given a specific object, we first try to touch it by gradually inflating the full-length gripper if not $\Delta V_C < \delta_1$ and $\Delta V_F > \delta_2$. If $\Delta V_C < \delta_1$ and $\Delta V_F > \delta_2$, we assume that the gripper fully contacts the object and inflate it to a big pressure and lift it. If the inflation pressure reaches 30 kPa (a safe the pressure when the fingertips touch each other under free bending) without embracing the object, we reconfigure the gripper to a shorter effective length and repeat the same step until $\Delta V_C < \delta_1$ and $\Delta V_F > \delta_2$.

Table 1. Touch-reconfiguration-grasp flowchart.

1. Move the gripper on the top of the object
2. Set the gripper to effective length L_III
3. Increase the pressure with 5 kPa
4. **While** Inflation pressure $\leqslant$ 35 kPa
5. **if** not ($\Delta V_C < 0$ and $\Delta V_F > 0$)
6. Increase the pressure with 5 kPa
7. **else**
8. Touch succeed, lift the object
9. break
10. Reconfigure the gripper to effective length L_II
11. Increase the pressure with 5 kPa
12. **While** Inflation pressure $\leqslant$ 35 kPa
13. **if** not ($\Delta V_C < 0$ and $\Delta V_F > 0$)
14. Increase the pressure with 5 kPa
15. **else**
16. Touch succeed, lift the object
17. break
18. Reconfigure the gripper to effective length L_I
19. Increase the pressure with 5 kPa
20. **While** Inflation pressure $\leqslant$ 35 kPa
21. **if** not ($\Delta V_C < 0$ and $\Delta V_F > 0$)
22. Increase the pressure with 5 kPa
23. **else**
24. Touch succeed, lift the object
25. break

We try to grip an octagonal prism to showcase the value of controlling VEL of the actuator during the autonomous closed-loop control. The demonstration of the strategy is shown in figure 5(a). As the picture on the left shows, when the gripper tries to touch the object with its full-length, the tip of the gripper does not touch the object. The sensor outputs $\Delta V_C < \delta_1$ and $\Delta V_F = 0$, also indicating this trial is failed. After cooling and reheating process, the gripper reconfigures to a shorter effective length (L_I as the inset infrared image shows), which took about 15 s in total. After reconfiguration, we use the gripper to grasp the object again. For this trial, the right picture shows that the tip of the gripper fully touches the object. The successful trial is also verified by $\Delta V_C < \delta_1$ and $\Delta V_F > \delta_2$. (The touch-reconfiguration- grasp process is also demonstrated in supplementary video S8.) With the cooperation of the VEL and the sensing ability, the gripper can select an appropriate grasping strategy for a specific object, instead of a uniform grasping mode.

In the future, we envision that establishing a more concrete mathematical model that exploits the data of the sensors to automatically change the effective length would further complement the prototype for working under the unconstructed environment without visual feedback.

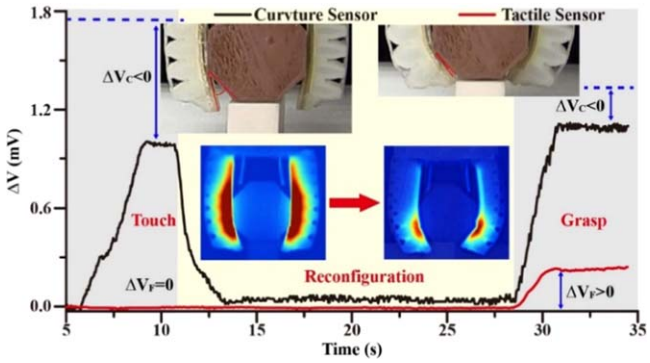

Figure 5. The touch-reconfiguration-grasp strategy demonstration. First, the gripper touches the octagonal prism under the fully softened state. The $\Delta V_C < \delta_1$ and $\Delta V_F = 0$ reveal that the grasp failed (also proved by the left figure, where the tip of the gripper does not touch the object). Then the gripper reconfigures to L_I with cooling and reheating process and grasps the object again. The $\Delta V_C < \delta_1$ and $\Delta V_F > \delta_2$ shows that the object is successfully conformed to the gripper. The right panel where the tip of the gripper touches the object can also prove it.

4. Conclusion

In summary, this paper reports a soft gripper with the ability of VELs and sensory feedback attribute to the combination of SMP and liquid metal. The fast softening and cooling method is proposed to improve the efficiency of the gripper. With the built-in flexible heater, the VEL layer can finish the phase transition within about 0.6 s. And it takes about 14 s for the VEL layer to recover to the rigid state by using the vortex tube to improve the heat convection. By adjusting the effective length, the grasping space of the gripper can be adjusted to be similar to the size of the object so that the gripper would apply more force. With the feedback of the curvature sensor and tactile sensor, the gripper could sense the curvature change while sliding over the object, also the shape of the object via the slide- pinch and rotatory-pinch approaches. Under the cooperation of sensor feedback and VEL, the gripper can reconfigure the finger length for a specific object based on the sensor feedback during the touch trial. With the benefit of the integration of smart materials, our approach may confer the soft gripper embedded intelligence and improved functionalities. We envision that establishing a machine learning-based algorithm that exploits the sensory data to smartly choose appropriate finger configurations would further complement the idea, especially for the unconstructed environment.

5. Experimental section

For the experiments, we established a control system to inflate the gripper, and export cold air, as well as acquire the data from the two sensors. The details of the system are explained in figure S6.

5.1. Heating and cooling speed test

To test the phase transition speed of the VEL layer, the prototype was suspended in the air to reduce the heat conduction with the surroundings and coated with a black coating to diminish the light reflection. Then the constant current supplied by the DC power (MS605D, Maisheng, China) was energized to the pads of the heater. During the heating process, an infrared camera (Ti400, Fluck Thermography, USA) right above the prototype recorded the temperature change of the layer at a frame rate of 9Hz. Then the videos were processed with the software (SmartView 4.1, Fluck Thermography, USA) to obtain the temperatures at the time sequence. For this test, only the L_I section was tested because all the sections of the heater have the same structural design. Four constant currents (from 0.4 to 1 A with an interval of 0.2 A) were galvanized to the heater. And each current was tested three times to obtain the average phase transition time. For the cooling test, the VEL layer was first heated above the glass transition temperature, then the infrared camera recorded the cooling time under two conditions. One was to let the prototype cool in the natural condition, the other was to record the temperature after applying the cold air to the surface of the prototype via the vortex tube. Three trials were conducted for each condition.

5.2. Pull-off force test

The setup for the pull-off force test is shown in figure S7. The gripper was fixed to the clamp. The object (three cylinders with the diameter of 38, 48 and 58 mm separately for this experiment) was fastened to the force transducer (Mini 40 F/T sensor, ATI, USA) via the connector and the force transducer was mounted to the robot arm (MOTOMAN MH3F, YASKAWA Inc., Japan). During the test, the gripper was first heated to set the corresponding effective length (L_I, L_II and L_III), then inflated with a pressure of 40 kPa via the electric proportional valve (ITV0030, SMC, Japan) to encompass the object. After that, the gripper was moved upwards at a speed of 2 mm s^{-1} until it detached from the object. The force data during the whole process was recorded via the NI data acquisition board (PCI-6284, National Instruments, USA) at a frequency of 500 Hz. For each object, the three effective lengths were tested three times to obtain an average.

5.3. Tactile sensor and curvature sensor calibration

The experimental setup to calibrate the tactile sensor was shown in figure S8. The tactile sensor was kept still by fixing it to the desk via an adhesive tape. The sensor was connected to the precision digital multimeter (Fluke 8845A, Fluke Inc., USA) which can precisely measure the resistance. A rigid stamp with a diameter of 9 mm was fixed to the ATI transducer. During the test, the robot arm was first moved to let the stamp connect to the surface of the tactile sensor but not to press it. Then the robot arm was programmed to move downwards at a step of 0.03 mm and a speed of 0.3 mm s^{-1} to press the sensor. After a pause of 4 s, the robot arm repeated the step until it finally moved 0.3 mm. The force data were

recorded via the NI board and the resistance change was recorded via the Fluke 8845A. By mapping the force and the resistance at the same time, we figured out the relationship between the force and resistance. Three trials were conducted for the calibration. To calibrate the curvature sensor, we fixed the actuator to the clamp. After softening the corresponding effective lengths, the actuator was inflated with air pressure from 3 to 60 kPa with an interval of 3 kPa in free bending. The voltage change of the sensor at different pressures was recorded then converted to resistance variation. Three trials were conducted for this experiment and we used the control system to inflate the actuator and acquire the sensor data.

5.4. Sensor dynamic test

To test the dynamic response of the tactile sensor, we fixed the actuator to a base and blocked the displacement of the actuator using a block (as shown in the picture in figure 4). After softening the length L_II, the actuator was inflated with the pressure to execute different functions to test the response, hysteresis, repeatability, and sensitivity of the sensors. Here, we programmed the step function, square wave function, and triangular wave functions to test the sensor. To test the dynamic response of the curvature sensor, the actuator was programmed to bend in free space, performing the function of step increasing-decreasing, and sine wave.

Acknowledgments

This work was supported by the National Science Foundation support projects, China (Grant No. 61 633 004), in part by the National Key R&D Program of China (Grant No. 18YFB1304600), and National Science Foundation support projects 61 822 303, 91 848 105. We thank Ms. Adela Contreras for helping us revise the paper.

ORCID iDs

Yufei Hao https://orcid.org/0000-0002-5194-8999
Zemin Liu https://orcid.org/0000-0002-9211-6603
Jiaqi Liu https://orcid.org/0000-0003-2958-9309
Xi Fang https://orcid.org/0000-0002-3202-8708
Bin Fang https://orcid.org/0000-0002-9149-7336
Yingchun Guan https://orcid.org/0000-0002-6897-6064
Li Wen https://orcid.org/0000-0002-1498-3103

References

[1] Melchiorri C and Kaneko M 2008 *Springer Handbook of Robotics* vol 345 (Berlin: Springer)
[2] Aukes D M, Heyneman B, Ulmen J, Stuart H, Cutkosky M R, Kim S, Garcia P and Edsinger A 2014 *Int. J. Robot. Res.* **33** 721
[3] Shintake J, Cacucciolo V, Floreano D and Shea H 2018 *Adv. Mater.* **30** 1707035
[4] Lau G K, Heng K R, Ahmed A S and Shrestha M 2017 *Appl. Phys. Lett.* **110** 182906
[5] Shian S, Bertoldi K and Clarke D R 2015 *Adv. Mater.* **27** 6814
[6] Shintake J, Schubert B, Rosset S, Shea H and Floreano D 2015 *IEEE/RSJ Int. Conf. Intelligent Robots and Systems (Hamburg, Germany)* (Piscataway, NJ: IEEE) p 1097
[7] McCoul D, Rosset S, Besse N and Shea H 2016 *Smart Mater. Struct.* **26** 025015
[8] Firouzeh A and Paik J 2017 *Smart Mater. Struct.* **26** 055035
[9] Li H, Go G, Ko S Y, Park J O and Park S 2016 *Smart Mater. Struct.* **25** 027001
[10] Do T N, Phan H, Nguyen T Q and Visell Y 2018 *Adv. Funct. Mater.* **28** 1800244
[11] Niu D, Jiang W, Ye G, Lei B, Luo F, Liu H and Lu B 2019 *Smart Mater. Struct.* **28** 02LT01
[12] Abdullah A M, Li X, Braun P V, Rogers J A and Hsia K J 2018 *Adv. Mater.* **30** 1801669
[13] Zheng S Y, Shen Y Y, Zhu F B, Yin J, Qian J, Fu J Z, Wu Z L and Zheng Q 2018 *Adv. Funct. Mater.* **28** 1803366
[14] Pilz da Cunha M, Foelen Y, Van Raak R J H, Murphy J N, Tom A P, Debije M G and Schenning A P H J 2019 *Adv. Opt. Mater.* **7** 1801643
[15] Terryn S, Brancart J, Lefeber D, Van Assche G and Vanderborght B 2017 *Sci. Robot.* **2** eaan4268
[16] Liu Y, Zhang Y and Xu Q 2016 *IEEE/ASME Trans. Mechatron.* **22** 476
[17] Xu Q 2015 *IEEE Trans. Autom. Sci. Eng.* **14** 1415
[18] Zhang X and Xu Q 2019 *Precis. Eng.* **56** 53
[19] Polygerinos P, Wang Z, Overvelde J T, Galloway K C, Wood R J, Bertoldi K and Walsh C J 2015 *IEEE Trans. Robot.* **31** 778
[20] Mosadegh B, Polygerinos P, Keplinger C, Wennstedt S, Shepherd R F, Gupta U, Shim J, Bertoldi K, Walsh C J and Whitesides G M 2014 *Adv. Funct. Mater.* **24** 2163
[21] Hao Y, Gong Z, Xie Z, Guan S, Yang X, Wang T and Wen L 2018 *J. Bionic Eng.* **15** 220
[22] Polygerinos P, Wang Z, Galloway K C, Wood R J and Walsh C J 2015 *Robot. Auton. Syst.* **73** 135
[23] Yuk H, Lin S, Ma C, Takaffoli M, Fang N X and Zhao X 2017 *Nat. Commun.* **8** 14230
[24] Galloway K C, Becker K P, Phillips B, Kirby J, Licht S, Tchernov D, Wood R J and Gruber D F 2016 *Soft Robot.* **3** 23–33
[25] Zhao H, O'Brien K, Li S and Shepherd R F 2016 *Sci. Robot.* **1** eaai7529
[26] Ozel S, Keskin N A, Khea D and Onal C D 2015 *Sensors Actuators* A **236** 349
[27] Atalay A, Sanchez V, Atalay O, Vogt D M, Haufe F, Wood R J and Walsh C J 2017 *Adv. Mater. Technol.* **2** 1700136
[28] Bilodeau R A, White E L and Kramer R K 2015 *IEEE/RSJ Int. Conf. Intelligent Robots and Systems (Hamburg, Germany)* (Piscataway, NJ: IEEE) 2324
[29] Morrow J, Shin H S, Phillips-Grafflin C, Jang S H, Torrey J, Larkins R, Dang S, Park Y L and Berenson D 2016 *IEEE Int. Conf. Robotics and Automation (Stockholm, Sweden)* (Piscataway, NJ: IEEE) p 5024
[30] Truby R L, Wehner M, Grosskopf A K, Vogt D M, Uzel S G, Wood R J and Lewis J A 2018 *Adv. Mater.* **30** 1706383
[31] Zhang Y F, Zhang N, Hingorani H, Ding N, Wang D, Yuan C, Zhang B, Gu G and Ge Q 2019 *Adv. Funct. Mater.* **29** 1806698
[32] Li Y, Chen Y, Yang Y and Wei Y 2017 *IEEE Trans. Robot.* **33** 446
[33] Santoso J, Skorina E H, Salerno M, de Rivaz S, Paik J K and Onal C D 2019 *Smart Mater. Struct.* **28** 035012
[34] Hao Y, Wang T, Xie Z, Sun W, Liu Z, Fang X, Yang M and Wen L 2018 *J. Micromech. Microeng.* **28** 024004

[35] Zhou J, Yi J, Chen X, Liu Z and Wang Z 2018 *IEEE Robot. Autom. Lett.* **3** 3379
[36] Park Y L, Chen B R and Wood R J 2012 *IEEE Sens. J.* **12** 2711
[37] Wang C, Sim K, Chen J, Kim H, Rao Z, Li Y, Chen W, Song J, Verduzco R and Yu C 2018 *Adv. Mater.* **30** 1706695
[38] Zhao R, Yao Y and Luo Y 2016 *J. Med. Devices* **10** 021002
[39] Wang Q, Yu Y, Yang J and Liu J 2015 *Adv. Mater.* **27** 7109
[40] Li B, Gao Y, Fontecchio A and Visell Y 2016 *Smart Mater. Struct.* **25** 075009